A PHM Approach to Additive Manufacturing Equipment Health Monitoring, Fault Diagnosis, and Quality Control

Jae Yoon[1], David He[2], and Brandon Van Hecke[3]

[1,2,3]*University of Illinois at Chicago, Chicago, IL, 60607, USA*
jyoon52@uic.edu
davidhe@uic.edu
bvanhe2@uic.edu

ABSTRACT

Fabrication of three-dimensional (3D) objects through direct deposition of functional materials using 3D printing equipment is called additive manufacturing (AM). Benefits of AM include producing goods quickly and on-demand, with greater customization and complexity and less material waste. While the use of AM has been growing, a number of challenges continue to impede its more widespread adoption, particularly in the areas of non-destructive evaluation/non-destructive testing (NDE/NDT) techniques for AM equipment health monitoring and measurement. In this paper, a prognostics and health management (PHM) approach to AM equipment health monitoring, fault diagnosis and quality control is presented and illustrated with a case study. The presented PHM approach is developed using two types of NDE/NDT sensors: acoustic emission (AE) sensor and piezoelectric strain sensor. A seeded driving belt fault on a fused filament fabrication desktop 3D printer is used to validate the feasibility of the PHM approach in the case study. The case study results have shown the effectiveness of the presented method for AM equipment fault diagnosis and quality control.

1. INTRODUCTION

In his 2013 state of the union address, US President Obama called three-dimensional (3D) printing "the potential to revolutionize the way we make almost everything" (Office of the Press Secretary, 2013). Fabrication of 3D objects through direct deposition of functional materials using 3D printing equipment is called additive manufacturing (AM). Benefits of AM include producing goods quickly and on-demand, with greater customization and complexity and less material waste. If the modern manufacturing which was subtractive process by cutting or milling is optimized at mass production, the future manufacturing would be called a creative customization through 3D printing at consumers' will.

While the use of AM has been growing, a number of challenges continue to impede its more widespread adoption, particularly in the areas of non-destructive evaluation/non-destructive testing (NDE/NDT) techniques for AM equipment health monitoring and measurement. According to a recent report on measurement science roadmap for metal-based additive manufacturing (Energetics Incorporated, 2013), current technical barriers or challenges in AM were roughly categorized as materials, process and equipment, qualification and certification, and modeling and simulation. Particularly in the process and equipment category, the highest priority in NDE/NDT techniques have been specified as: (1) Combining NDE techniques to better assess quality via an integrated approach; (2) Adapting existing NDE techniques to AM, especially parts, and characterizing defects; (3) Lack of affordable quality inspection tools for direct metal parts. Even though the 3D printing technology has been available since 80s, it was not until recent days that 3D printing came to the fore in commercial manufacturing. Thus, very few studies have been conducted on NDE based 3D printer health monitoring and prognostics. The AM has two unique characteristics: (1) relatively long cycle time; (2) high quality standard for dimension accuracy. These unique characteristics of AM can be considered as good opportunities for developing PHM based approach for 3D printer health monitoring, fault detection and quality control. As the dimension accuracy of the printed product can be caused by inaccurate movement of the 3D printer, by detecting the 3D printer fault and stopping the faulty execution of the printing process, manufacturing time, materials, and cost can be saved and product quality assured.

In the related field of rotating machinery fault detection and diagnostics, the use of different NDE/NDT techniques such as acoustic emission (Yoshioka and Fujiwara, 1984; Tandon and Mata, 1999; Tandon and Narka, 2000; Scheer *et al*.,

2007; Bechhoefer *et al.*, 2013; Qu *et al*., 2013 and 2014), torsional vibration (Feng & Zuo, 2013), and fiber optic strain sensors (Kiddy *et al*., 2011) has been investigated with drivetrain in wind turbine and rotorcraft. In this study, the potential capability of acoustic emission (AE) and piezoelectric (PE) strain sensors as fault detection and quality control technique for AM equipment and product is investigated.

AE is commonly defined as transient elastic waves within a material, caused by the release of localized stress energy (Mathews, 1983). The advantage of using AE sensor as failure analysis source is that AE propagates from the epicenter to sensing apparatus within materials while vibration sensor requires perpendicular installation along with the vibration direction. Identifying vibration direction is sometimes painful if their sources are combinative. Also, AE signals are distinguishable from acoustic signals in that acoustic signals generally lie on the audible range of human (*e.g.* 20 Hz ~ 20 kHz). On the other hand, AE signals lie on a higher frequency range (*e.g.* 1 kHz ~ 1 MHz). Thus a high sampling rate between 2 to 10 MHz has been a typical choice of sampling rate for AE data collection. Other issues may arise including a high data volume and complicated feature of AE signals, which make the AE data processing challenging. However, it has been also reported that AE sensors are more sensitive in early fault detection than vibration sensors with various gear and bearing fault diagnostic applications (Yoshioka and Fujiwara, 1984; Tandon and Mata, 1999; Tandon and Narka, 2000; and Scheer *et al*., 2007).

The feasibility of using fiber optic strain sensors to detect damaged gearbox was recently reported by Kiddy *et al*. (2011). In their study, fiber optic strain sensors were mounted on a helicopter transmission test rig to investigate the detectability of gear fault conditions. However, the low maximum sampling rate (up to 1 kHz) of the fiber optic strain sensor limits its wide applicability in machinery fault detection. On the other hand, the PE strain sensors measure torsional vibration by quantifying terminal voltage difference released by deformed piezoelectric material. Unlike the fiber optic strain sensor, PE strain sensor has a merit in higher sampling rate up to 100 kHz. Compared to the conventional strain gauge sensors and accelerometers, the PE strain sensors have certain advantages that could be summarized as follows: (1) ability to measure the first derivative of physical deformation, (2) high linearity and sensitivity from their superior noise immunity as compared to differentiated sensing performance of conventional strain sensors (Lee and O'Sullivan, 1991; Banaszak 2001), (3) high frequency range (Jiang *et al.*, 2014), (4) space-efficiency without a structural change on the measuring target (Kon *et al*., 2007), and (5) negligible temperature effect on the measurement output (Sirohi and Chopra, 2000; Jiang *et al.*, 2014). The aforementioned benefits allow PE strain sensors to potentially have greater sensing resolution and accuracy.

Up to today, no investigation on 3D printer health monitoring and fault diagnosis has been reported in the literature. In this paper, an investigation into the feasibility of PHM based AE and PE strain signal analysis techniques for 3D printer fault detection and quality control is reported. The remainder of the paper is organized as follows. Section 2 provides a detailed explanation of the proposed methodology. In Section 3, the details of the experimental setup and the seeded fault tests on a 3D printer test rig for validating the proposed methodology are provided. Section 4 presents the 3D printer fault detection results from the seeded fault tests. Finally, Section 5 concludes the paper.

2. METHODOLOGY

An overview of the proposed methodology is provided in Figure 1. As shown in Figure 1, a data acquisition (DAQ) system is used to collect the AE signals and PE strain signals at the same time. While the PE sensor is directly connected to the DAQ, the AE sensor, on the other hands, is connected to the DAQ board through a hardware based heterodyne frequency reduction device. Then, filter bands are chosen for each sensor to remove noise in the collected signals before they can be used to compute condition indicators (CIs) for fault detection. The key components of the methodology are explained in the next two sections. Section 2.1 provides a brief review of the hardware based heterodyne technique for AE sensor and the computation of CIs for 3D printer fault detection is followed in Section 2.2.

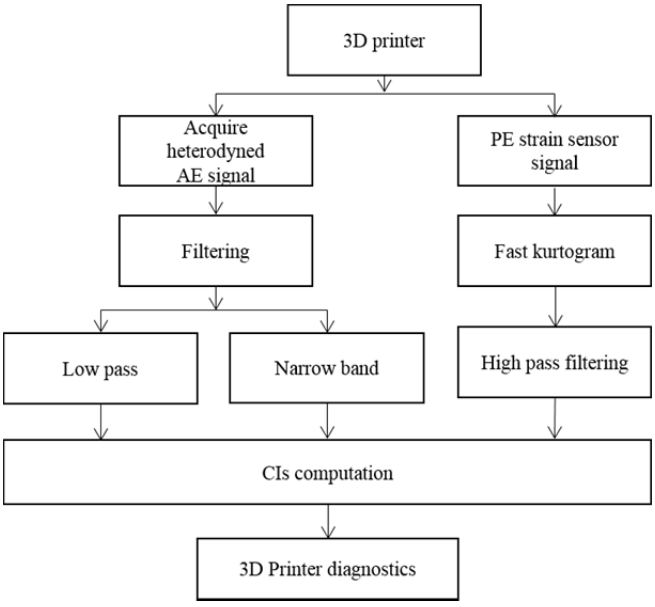

Figure 1. Overview of the 3D printer fault diagnosis with PE strain sensor and AE sensor.

2.1. The Heterodyne Technique

To apply AE based NDE/NDT techniques to machine fault detection and diagnosis, one technical challenge is to deal with the data storage and processing burden caused by the typical high sampling rate of AE sensor (from several MHz to 10 MHz). To meet the challenge, frequency shifting technique, namely heterodyne (Fessenden, 1913) based AE fault detection and diagnosis methods have been developed for gearboxes (Bechhoefer *et al.*, 2013; Qu *et al.*, 2013; 2014). The heterodyne technique downshifts the frequency of the AE signals so that a sampling rate comparable to vibration analysis can be utilized. Qu *et al.* (2013 and 2014) have shown the effectiveness AE based fault detection and diagnosis using heterodyne technique with a sampling rate as low as to 20 kHz for a split torque type gearbox. The AE based NDE/NDT techniques implemented with heterodyne are significant as size of AE data needs to be stored and the computational cost can be significantly reduced. The heterodyned AE technique implemented in this paper works similarly to a radio quadrature demodulator: shifting the carrier frequency to baseband, followed by low pass filtering. Mathematically, heterodyning is based on the trigonometric identity. For two signals with different frequency f_1 and f_2, respectively, their product could be written as:

$$\sin(2\pi f_1 t)\ \sin(2\pi f_2 t) = \frac{1}{2}\cos[2\pi(f_1 - f_2)] - \frac{1}{2}\cos[2\pi(f_1 + f_2)] \quad (1)$$

where f_1 is the AE carrier frequency and f_2 is the demodulator's reference signal frequency. In applications, any desired new output signals called as heterodynes, one at the sum $f_1 + f_2$, and the other at the difference $f_1 - f_2$, are utilized upon necessity. Technically, the heterodyning technique is aimed especially at demodulating the amplitude modulated signals. The amplitude modulation process can be mathematically expressed as:

$$U_a = (U_m + mx)\cos\omega_c t \quad (2)$$

where, U_a is the amplitude modulated signal, U_m is the carrier signal amplitude, m is the modulation coefficient, x is the signal of interest, and ω_c is the carrier signal frequency. By introducing an amplitude and frequency for x by X_m and Ω, respectively, the signal of interest x can be represented as:

$$x = X_m cos\Omega t \quad (3)$$

Note that it is assumed that Ω is much smaller than ω_c. Then, with the heterodyning technique, the modulated signal will be multiplied by a unit amplitude reference signal $\cos(\omega_c t)$. Then the resulting U_o can be written as:

$$U_o = (U_m + mx)\cos(\omega_c t)\cos(\omega_c t) = (U_m + mx)\left[\frac{1}{2} + \frac{1}{2}\cos(2\omega_c t)\right] \quad (4)$$

Substituting Eq. (3) into Eq. (4) yields:

$$U_o = \frac{1}{2}U_m + \frac{1}{2}mX_m cos\Omega t + \frac{1}{2}U_m cos(2\omega_c t) + \frac{1}{4}mX_m[cos(2\omega_c + \Omega)t + cos(2\omega_c - \Omega)t] \quad (5)$$

Since U_m is assumed not to contain any useful information related to the modulated signal, it could be canceled out. From Eq. (5), it can be concluded that only the second term $\frac{1}{2}mX_m cos\Omega t$ will remain after applying low pass filter, while the high frequency components around frequency $2\omega_c$ will be removed. In the final heterodyning demodulation step, the signal frequency can be reduced to 10s of kHz. The resulting frequency range for AE signals becomes comparable to that of typical vibration signals. Thus, a lower sampling rate in an AE data acquisition system can be used. The heterodyned AE data acquisition procedure is shown by comparing it with the conventional AE method in Figure 2.

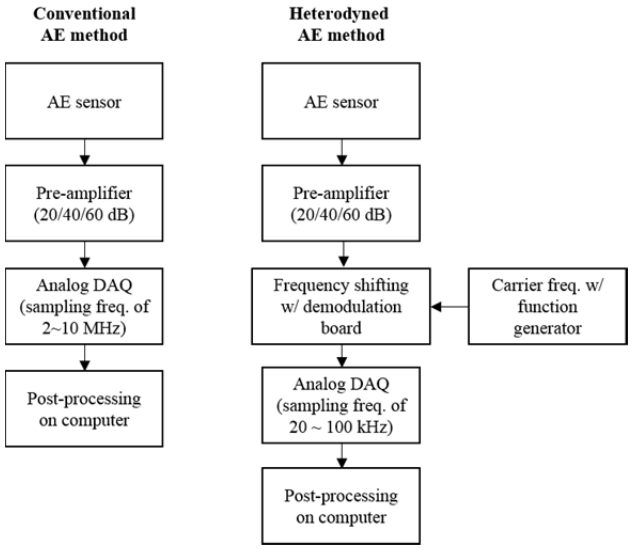

Figure 2. Comparison of the heterodyned AE data acquisition procedure with the conventional AE methods.

Finding a proper reference signal is critical to the successful implementation of the heterodyne technique in AE data acquisition. Since each AE sensor product from varying manufacturers has a unique frequency characteristic, the following optimization process based a linear chirp function is performed so that the root mean square (RMS) of the demodulated output signal could be maximized. The optimization process is described in Qu *et al.* (2014).

2.2. CIs for 3D Printer Fault Detection

Table 1 provides the definitions of CIs investigated for 3D printer fault detection in this paper. The CIs can be defined into five general types: root mean square (*RMS*), peak to

Table 1. The definitions of the CIs.

		Input Signal (x_{IN})				
		Raw AE	EO	NB	AM	FM
CI	Description / Equation	Raw heterodyned AE data (x_{raw})	Energy operator: a residual of the autocorrelation function (x_{EO})	Narrow band pass filtered (x_{NB})	Amplitude modulation of NB filtered signal ($AM(x_{NB})$)	Frequency modulation of NB filtered signal ($FM(x_{NB})$)
Root mean square (*RMS*)	$RMS(x_{IN}) = \sqrt{\frac{1}{N}\sum_{i=1}^{N} x_i^2}$	$RMS(x_{IN})$: measures the magnitude of a discretized signal.				
Peak to peak (*P2P*)	$P2P(x_{IN}) = \frac{(\max(x_{IN}) - \min(x_{IN}))}{2}$	$P2P(x_{IN})$: measures the maximum difference within the data range.				
Skewness (*SK*)	$SK(x_{IN}) = \frac{\frac{1}{N}\sum_{i=1}^{N}(x_i - \bar{x})^3}{\left[\sqrt{\frac{1}{N}\sum_{i=1}^{N}(x_i - \bar{x})^2}\right]^3}$	$SK(x_{IN})$: measures the asymmetry of the data about its mean value. A negative *SK* value and positive *SK* value imply the data has a longer or fatter left tail and the data has a longer or fatter right tail, respectively.				
Kurtosis (*KT*)	$KT(x_{IN}) = \frac{N\sum_{i=1}^{N}(x_i - \bar{x})^4}{\left[\sum_{i=1}^{N}(x_i - \bar{x})^2\right]^2}$	$KT(x_{IN})$: measures the peakedness, smoothness, and the heaviness of tail in a data set.				
Crest factor (*CF*)	$CF(x_{IN}) = \frac{P2P(x_{IN})}{RMS(x_{IN})}$	$CF(x_{IN})$: measures the ratio between $P2P(x_{IN})$ and $RMS(x_{IN})$ to describe how extreme the peaks are in a waveform.				

Note: x_i is i^{th} element of the input data x_{IN}; N is the length of the input data x_{IN}; max(·) returns the maximal element of input data x_{IN}; min(·) returns the minimal element of input data x_{IN}; $\bar{x}$ is a mean value of the input data x_{IN} defined as $\sum_{i=1}^{N} x_i / N$

peak (*P2P*), skewness (*SK*), kurtosis (*KT*), and crest factor (*CF*). Each type of CI can be computed using different input signals. In addition to raw signals, other types of input signals can be generated: energy operator (EO), narrow band (NB), AM, and FM. The EO introduced by Teager (1992) is defined as the residual of the autocorrelation function as following:

$$x_{EO,i} = x_i^2 - x_{i-1} \cdot x_{i+1}, \quad (\text{for } i = 2, 3, \dots, N-1) \tag{6}$$

where $x_{EO,i}$ is the i^{th} element of EO data; x_i is the i^{th} element of the input data x_{IN}. NB is the time domain representation after applying narrow band of interest which could be seen in frequency domain. Finally, AM and FM are obtained by amplitude modulation and phase modulation of the NB filtered data.

3. EXPERIMENTAL SETUP

This section covers the experimental setup used to establish the AE and PE strain sensor based 3D printer fault diagnosis technique. The methodologies were validated with a desktop 3D printer using fused filament fabrication. Section 3.1 introduces the 3D printer test rig and Section 3.2 covers the seeded fault test.

3.1. The 3D Printer Test Rig

Figure 3 shows the 3D printer test rig and the DAQ system used in the seeded fault test in this paper.

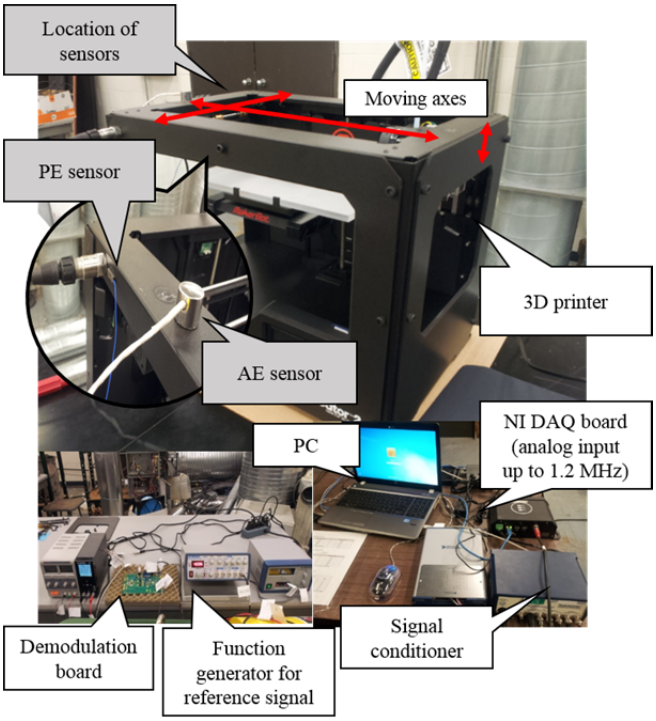

Figure 3. The 3D printer test rig and the DAQ system.

The 3D printer test rig composes two main parts: (1) heterodyned AE based DAQ system, (2) 3D printer. The DAQ system includes a National Instruments' DAQ board with a maximum analog input sampling rate of 1.25 MHz, AE sensor attached on the 3D printer, demodulation board (AD8339), analog amplifier with gain 20/40/60dB, and function generator. The 3D printer (Makerbot, 2014) has a layer resolution up to100 µm, position precision of 11 µm on *X* and *Y* axes and 2.5 µm on *Z* axis, and a nozzle of 0.4 mm diameter controlled by two stepper motors and wear resistant oil-infused bronze bearings.

3.2. 3D Printer Seeded Fault

According to the troubleshooting maintenance document (Makerbot, 2014) of the machine, one potential problem is the looseness of the belt driving the motion of the extruder nozzle. Thus, a malfunctioned toothed belt scenario was artificially created and simulated in this paper. The seeded fault was created by inserting five small pieces of metal wire into the slots between teeth of belt to create faulty operation during printing process. Figure 4 shows the seeded fault created by inserting a metal wire piece into the slot between two teeth on the toothed driving belt to simulate the looseness of the driving belt. The inserted metal wire piece was cut into the same dimensions in size as the slot between the belt teeth so that the slot was perfectly filled with the metal wire piece. Then the metal wire piece was tied on the belt with a thin flexible tape.

Figure 4. Seeded fault on toothed belt.

The 3D printer was run with and without the fault seeded driving belt to produce ten sets of bolt and nut (five sets for each conditions). Individual run took about 28 minutes to print one set of bolt and nut. For sample consistency, a total of six heterodyned AE data samples were recorded for 10 seconds at pre-specified time locations from each run. The data acquisition procedure for the seeded fault test is depicted with a flowchart in Figure 5.

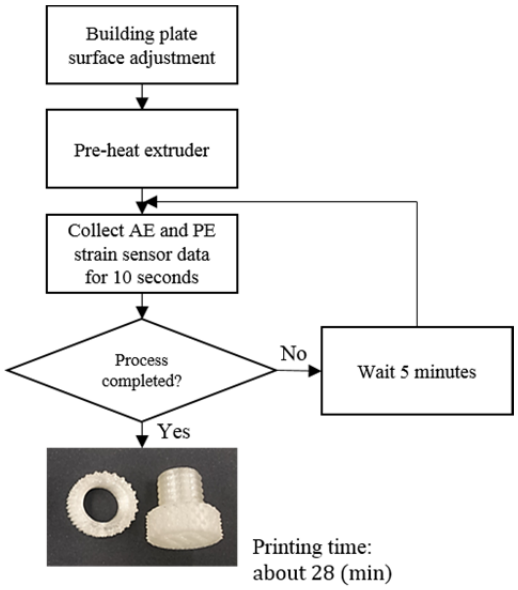

Figure 5. Data acquisition procedure.

Figure 6 shows the 3D outputs of the healthy and faulty 3D printers. Under the normal printing conditions, the printed nut and bolt should smoothly thread together and function as intended. Under the faulty printing condition, even though the pair of printed bolt and nut appears to be normal, the bolt can only be turned into the nut half way. This clearly indicates that the threads on the bolt or inside the nut

were not printed up to the required precision due to the driving belt fault in the 3D printer.

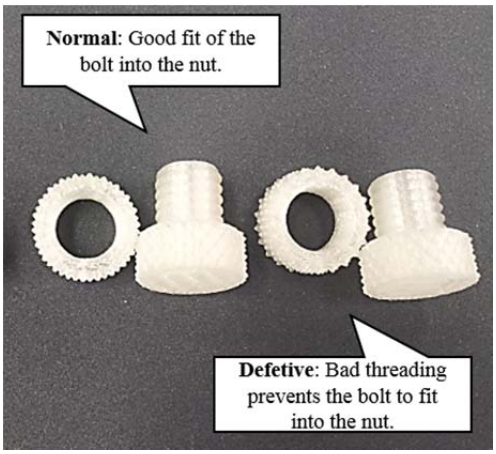

Figure 6. 3D outputs from the healthy and the faulty 3D printers.

4. RESULTS

This section covers the 3D printer fault diagnostic results from the AE and PE strain sensor based technique. Section 3.1 explains AE signal analysis results and Section 3.2 the PE strain sensor signal analysis results.

4.1. AE Signal Analysis Results

The AE signal analysis results for the seeded fault tests conducted on the 3D printer test rig are provided in this section. Figure 7 shows the spectrums of AE data samples. By examining the spectrums in Figure 7, two different frequency regions were chosen for the low pass and narrow band pass filters: low frequency region up to 20 kHz and narrow band frequency around 3906 Hz. As shown in Figure 7, a remarkably high peak was observed within low pass range from all of AE samples. These peaks are specifically located at 3906 Hz. So a narrow band pass filter with a band width of 3906±3 Hz around the peak frequency location was chosen.

In Figure 8, RMS result from the low pass filter is provided. The resulting RMS of the heterodyned AE sample showed clear separation between healthy and faulty 3D printing condition. In Figure 8(a), RMS values at each sample location and trial are presented. In Figure 8(b), the averaged RMS values with a 95% confidence interval at each sample location are provided.

In Figures 9 to 12, CIs from the narrow band filtered AE signals are provided. Among all the CIs tested, majority of those that show a clear separation between the healthy and faulty conditions were computed from narrow band filtered signals. Note that the bandwidth of this narrow band is in the low frequency filter region. A clear separation between the healthy and faulty 3D printing conditions with a 95% statistical significance can be observed for the following AE based CIs: RMS, NB-RMS, NB-P2P, AM-RMS, and AM-P2P.

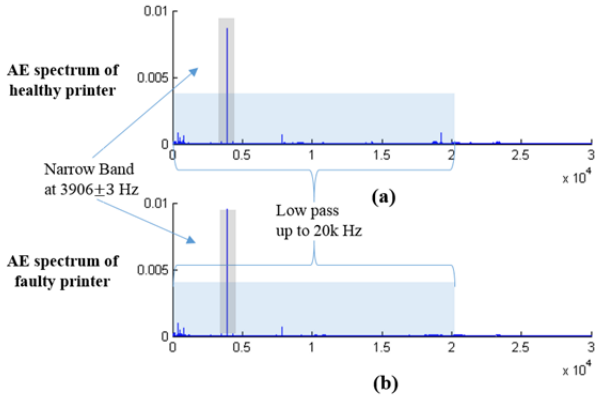

Figure 7. Spectrum of 3D printer AE signal samples: (a) healthy, (b) faulty.

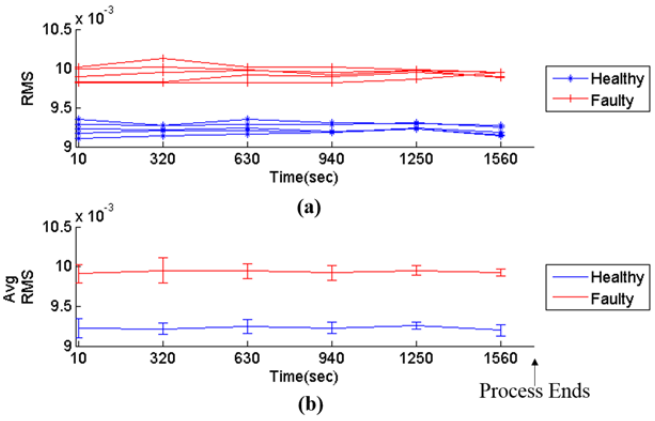

Figure 8. RMS of healthy and faulty low pass filtered results: (a) all data, (b) average with 95% confidence interval.

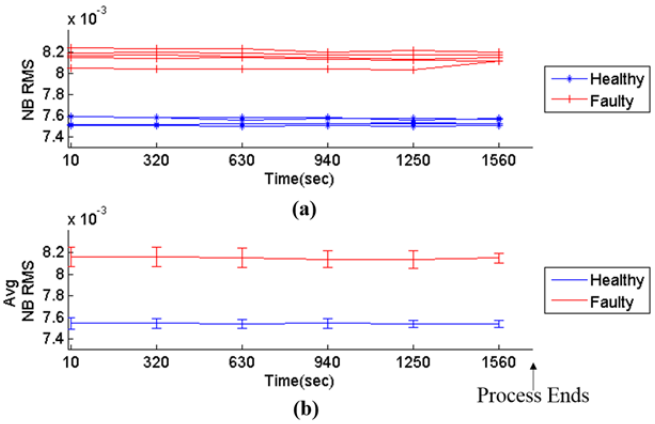

Figure 9. RMS from narrow band pass filtered result: (a) all data, (b) average with 95% confidence interval.

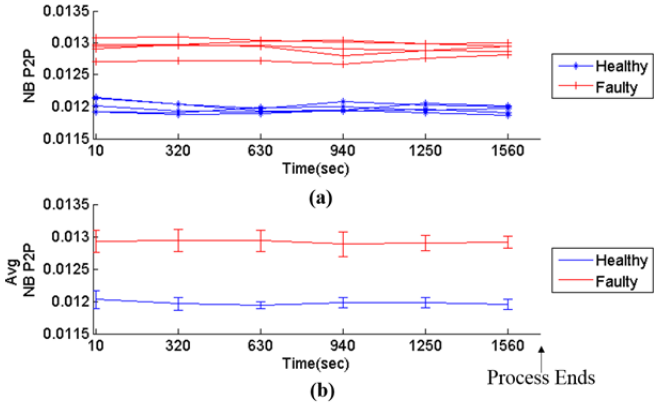

Figure 10. Peak to peak from narrow band pass filtered result: (a) all data, (b) average with 95% confidence interval.

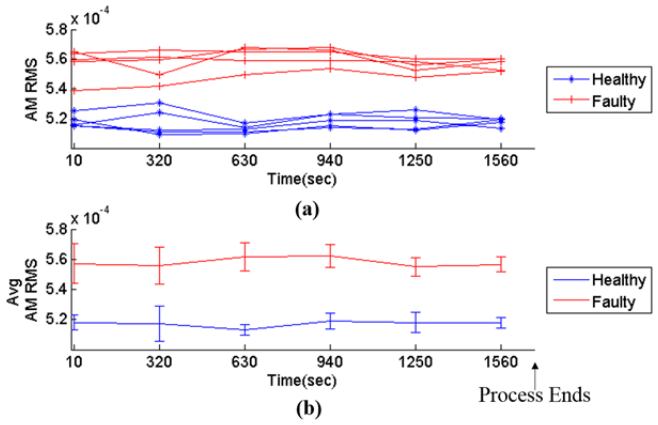

Figure 11. RMS from amplitude modulation result after narrow band pass filtered result: (a) all data, (b) average with 95% confidence interval.

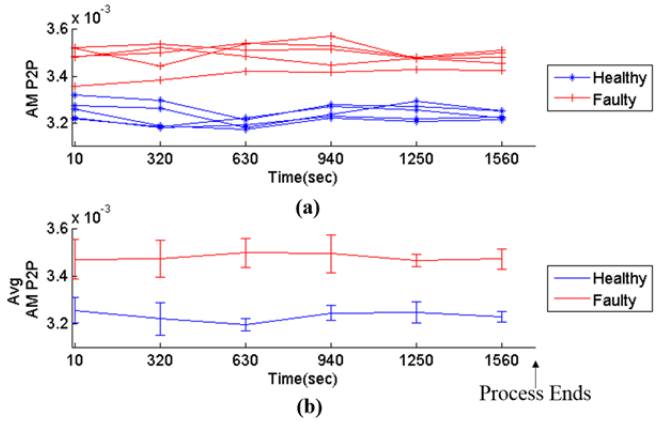

Figure 12. Peak to peak from amplitude modulation result after narrow band pass filtered result: (a) all data, (b) average with 95% confidence interval.

4.2. PE Strain Signal Analysis

In processing the PE strain sensor signals to extract CIs for the 3D printer fault detection, a similar strategy used by Kiddy *et al.* (2011) was applied. In their study, PE strain signals were divided into two parts based on their frequency: low frequency part and high frequency part. Actual damage detection was performed on the high frequency part of the strain sensor data using condition indicators. Thus, in this research, high pass filtered PE strain signals were used to compute the CIs. In search for the appropriate filter band, the fast kurtogram (Antoni, 2007) was applied to exam the impulsivity locations of PE strain signals collected from the healthy 3D printers.

Provided in Figure 13, a sample fast kurtogram result from the healthy 3D printer is displayed. The area in dark red color indicates the location of impulsivity. Statistical result of the fast kurtogram is summarized in Table 2. The 90% and 95% trimmed mean indicate that the impulsivity of PE sensor signals are located around 3.3 kHz to 4.2 kHz, respectively. Thus, a high pass band above 3 kHz was selected. Here a X % trimmed mean is the average of the data after $(100 - X)$% of the outliers are removed.

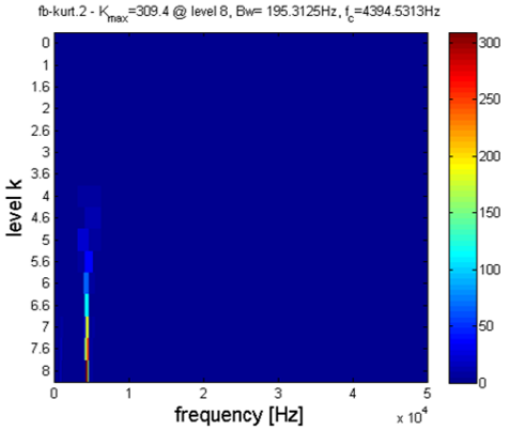

Figure 13. A sample fast kurtogram of PE strain sensor result from the healthy 3D printer.

Among all the CIs computed using PE strain signals, only RMS showed a clear separation of the faulty condition from the normal condition. The RMS of the PE stain signals and the averaged RMS with 95% confidence intervals for both the healthy and faulty conditions are provided in Figure 14.

Table 2. Statistical results of Fast kurtogram.

	Healthy	
	90% trimmed mean	95% trimmed mean
Center frequency value (Hz)	3320	4199

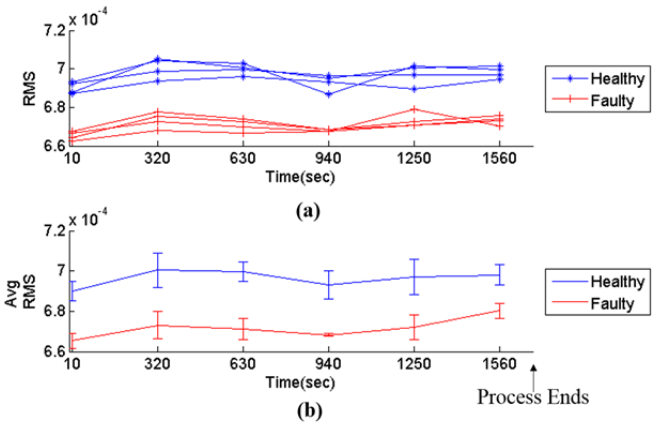

Figure 14. RMS of healthy and faulty PE strain signals: (a) all data, (b) average with 95% confidence interval.

4.3. Results Summary

The 3D printer seeded fault detection results using both the AE sensor and PE strain sensor can be summarized in Table 3.

Table 3. Summary of the 3D printer fault detection results using AE and PE strain sensors.

Sensor Type	AE Sensor		PE Strain Sensor
Sampling frequency	100 kHz		100 kHz
Filter bandwidth	Low pass band (< 20 kHz)	Narrow band (3906 ± 3 Hz)	High pass band (> 3k Hz)
Effective CIs selected	RMS	NB-RMS, NB-P2P, AM-RMS, AM-P2P	RMS

As shown in Table 2, for both the AE sensor and PE strain sensor used in the case study for 3D printer fault detection, a sampling rate of 100 kHz was used for data acquisition. For AE sensor signals, two band pass filters were used: a low pass filter and a narrow band filter. When the low pass filter was used, RMS provided the best performance and was able to detect the fault. When a narrow band filter was used, the following CIs were able to detect the fault: NB-RMS, NB-P2P, AM-RMS, and AM-P2P. For PE strain sensor signals, a high pass filter was used and only one CI, RMS, was able to detect the fault.

It has to be pointed out that the 3D printer fault was detected right after the first sample data was collected by both the AE and PE strain sensor in the seeded fault test. In real AM application, it can take up to several days to print out a product by a 3D printer. Therefore, significant amount of manufacturing time, materials, and cost can be saved and the quality of the product can be assured if a 3D printer fault can be detected and the printer be stopped days before it finishes printing the defective product.

5. CONCLUSIONS

In this paper, an investigation into the feasibility of PHM based AE and PE strain signal analysis techniques for 3D printer fault detection and quality control was reported. The presented PHM approach was developed using two types of NDE/NDT sensors: AE sensor and piezoelectric strain sensor. A seeded driving belt fault on a fused filament fabrication desktop 3D printer was used to validate the feasibility of the PHM approach in the case study. For the AE signal analysis in particular, a high peak in the frequency domain was detected and a narrow band pass filter around the peak was used to extract multiple condition indicators to detect the fault. On the other hand, in the PE strain analysis, the fast kurtogram was used to determine the proper high-pass filter band to obtain high frequency components to obtain effective fault detection CIs. The results have shown that the driving belt seeded looseness fault could be detected by both of the AE and PE strain sensor analysis methods. The methods presented in this paper could be extended to other potential 3D printing faults such as material feed or additional mechanical component faults.

REFERENCES

Antoni, J. (2007). Fast computation of the kurtogram for the detection of transient faults, *Mechanical Systems and Signal Processing*, Vol. 32, No. 1, pp. 108 - 124.

Banaszak, D. (2001). Comparison of piezoelectric strain sensors with strain gages, *Proceedings of the Annual Meeting of the American Statistical Association*, August 5 – 9, Atlanta, GA.

Bechhoefer, E., Qu, Y., Zhu, J., & He, D. (2013). Signal processing technique to improve an acoustic emission sensors, *Proceedings of the Annual Conference of the Prognostics and Health Management Society 2013*, October 14 – 17, New Orleans, LA.

Energetics Incorporated. (2013). Workshop summary report: measurement science roadmap for metal-based additive manufacturing, *National Institute for Standards and Technology (NIST)*, U.S. Department of Commerce, May 13.

Feng, Z. & Zuo, M. J. (2013). Fault diagnosis of planetary gearboxes via torsional vibration signal analysis, *Mechanical Systems and Signal Processing*, Vol. 36, No.2, pp. 401 - 421.

Fessenden, R. A. (1913). *Electric Signaling Apparatus*, US Patent 1050441A, January 14.

Lee, C. K. & O'Sullivan, T. (1991). Piezoelectric strain rate gages," *Journal of the Acoustical Society of America*, Vol. 90, No.2, pp.945 - 953.

Kiddy, J. S., Samuel, P. D., Lewicki, D. G., LaBerge, K. E., Ehinger, R. T., & Fetty, J. (2011). Fiber optic strain sensor for planetary gear diagnostics, *NASA Technical Report: NASA/TM-2011-217123*, NASA Glenn Research Center, Cleveland, OH.

Kon, S., Oldham, K., & Horowitz, R. (2007). Piezoresistive and piezoelectric MEMS strain sensors for vibration detection, *Proceedings of the SPIE: Sensors and Smart Structures Technologies for Civil, Mechanical, and Aerospace Systems*, Vol. 6529, pp. 1 - 11.

MakerBot Industries, LLC. (2014). *Replicator2 Desktop 3D Printer User Manual*, Brooklyn, NY.

Mathews, J. R. (1983). *Acoustic Emission*, Gordon and Breach Science Publishers Inc., New York, NY, USA.

Office of the Press Secretary. (2013). *Remarks by the President in the State of the Union Address*, February 12, 2013. http://www.whitehouse.gov/the-press-office/2013/02/12/remarks-president-state-union-address

Scheer, C., Reimche, W., & Bach, F.W. (2007). Early fault detection at gear units by acoustic emission and wavelet analysis, *Journal of Acoustic Emission*, Vol. 25, No. 1, pp. 331 – 340.

Sirohi, J. & Chopra, I. (2000). Fundamental understanding of piezoelectric strain sensors, *Proceedings of Journal of Intelligent Material Systems and Structures*, Vol. 11, No. 4, pp. 246 - 257.

Tandon, N. & Mata, S. (1999). Detection of defects in gears by acoustic emission measurements, *Journal of Acoustic Emission*, Vol. 17, No. 1-2, pp. 23 - 27.

Tandon, N. & Nakra, B. C. (2000). Comparison of vibration and acoustic measurement techniques for the condition monitoring of rolling element bearings, *Tribology International*, Vol. 25, No. 3, pp. 205 - 212, 1992.

Teager, H. M., & Teager S. M. (1992). Evidence for nonlinear sound production mechanisms in the vocal tract, , *Speech Production and Speech Modeling Symposium, Time Frequency and Time-Scale Analysis*, edited by Hardcastle, W. J. and Marchal, A., Springer, Amsterdam, Netherlands.

Qu, Y., He, D., Bechhoefer, E., & Zhu, J. (2013). A new acoustic emission sensor based gear fault detection approach, *International Journal of Prognostics and Health Management*, Vol. 4, Special Issue on Wind Turbine PHM, pp. 1 - 14.

Qu, Y., He, D., Yoon, J., VanHecke, B., Bechhoefer, E., & Zhu, J. (2014). Gearbox tooth cut fault diagnostics using acoustic emission and vibration sensors - a comparative study, *Sensors*, Vol. 14, No. 1, pp. 1372 - 1393.

Yoshioka, T., & Fujiwara, T. (1984). Application of acoustic emission technique to detection of rolling bearing failure, *American Society of Mechanical Engineers*, Vol. 14, No. 1, pp. 55 - 76.

BIOGRAPHIES

Jae Yoon received his B.E degree in Control engineering from Kwangwoon University, Republic of Korea, worked at Samsung Electronics Co. Ltd. as a product engineer from 2006 through 2008. He then received M.S. degree in Mechanical engineering from the University of Florida. He joined the Intelligent Systems Modeling & Development Laboratory in the department of Mechanical and Industrial Engineering at the University of Illinois-Chicago to pursue Ph.D. degree. His current research interests include: machinery health monitoring for CBM, data-driven methods for diagnostics, and model based and data mining based prognostics, encompassing reliability engineering.

David He Dr. He is a Professor and Director of the Intelligent Systems Modeling & Development Laboratory in the Department of Mechanical and Industrial Engineering at The University of Illinois-Chicago. Dr. He's research areas include: machinery health monitoring, diagnosis and prognosis, complex systems failure analysis, quality and reliability engineering, and manufacturing systems design, modeling, scheduling and planning.

Brandon Van Hecke received his B.S. in Industrial Engineering from the University of Illinois at Chicago in 2010. He is a Ph.D. candidate in the Department of Mechanical and Industrial Engineering. His research interests include digital signal processing, machinery health monitoring, bearing and gear fault diagnostics based on the evaluation of vibration and acoustic emission signals, and condition based maintenance.